American Mineralogist, Volume 88, pages 1542–1554, 2003

New clinopyroxene-liquid thermobarometers for mafic, evolved, and volatile-bearing lava compositions, with applications to lavas from Tibet and the Snake River Plain, Idaho

KEITH D. PUTIRKA,[1,*] HAIG MIKAELIAN,[2] FREDERICK RYERSON,[2] AND HENRY SHAW[2]

[1]California State University, Fresno, Department of Earth and Environmental Sciences, 2345 E. San Ramon Avenue, MS/MH24, Fresno, California 93720, U.S.A.

[2]Lawrence Livermore National Laboratory, Institute of Geophysics and Planetary Physics, Livermore, California 94566, U.S.A.

ABSTRACT

Our ability to calculate the depths and temperatures at which magmas partially crystallize can prove crucial as petrologists test hypotheses of magma transport and evolution. Yet whereas numerous magma transport arguments involve hydrous and SiO_2-rich volcanic products, current clinopyroxene-liquid thermobarometers have been calibrated only from basaltic liquid compositions. To remedy this deficiency, new thermobarometers have been calibrated using new experiments that include hydrated (water-undersaturated) and SiO_2-rich liquids ranging to 71.3 wt% SiO_2. As with prior models, the new calibrations are based on jadeite crystallization and jadeite-diopside + hedenbergite exchange equilibria:

$$P(\text{kbar}) = -88.3 + 2.82\times10^{-3}T(\text{K})\ln\left[\frac{[\text{Jd}^{\text{cpx}}]}{\left[\text{Na}^{\text{liq}}\text{Al}^{\text{liq}}\left(\text{Si}^{\text{liq}}\right)^2\right]}\right] + 2.19\times10^{-2}T(K) - 25.1\ln[\text{Ca}^{\text{liq}}\text{Si}^{\text{liq}}]$$
$$+7.03[\text{Mg}'^{\text{liq}}] + 12.4\ln[\text{Ca}^{\text{liq}}]$$

$$\frac{10^4}{T(\text{K})} = 4.60 - 4.37\times10^{-1}\ln\left[\frac{\left[\text{Jd}^{\text{cpx}}\text{Ca}^{\text{liq}}\text{Fm}^{\text{liq}}\right]}{\left[\text{DiHd}^{\text{cpx}}\text{Na}^{\text{liq}}\text{Al}^{\text{liq}}\right]}\right] - 6.54\times10^{-1}\ln[\text{Mg}'^{\text{liq}}] - 3.26\times10^{-1}\ln[\text{Na}^{\text{liq}}]$$
$$- 6.32\times10^{-3}[P(\text{kbar})] - 0.92\ln[\text{Si}^{\text{liq}}] + 2.74\times10^{-1}\ln[\text{Jd}^{\text{cpx}}]$$

Here, T is in Kelvins and P is in kbar. Jd^{cpx} is the mole fraction of jadeite in clinopyroxene, where pyroxene cations are calculated on the basis of 6 O atoms, and Jd is the lesser of Na or ^{VI}Al; remaining Al is used to form CaTs. $DiHd^{cpx}$ is the mole fraction of diopside + hedenbergite in clinopyroxene, calculated as the fraction of Ca remaining after forming CaTs (= ^{VI}Al – Jd), $CaTiAl_2O_6$ [= (^{IV}Al – CaTs)/2], and $CaCr_2SiO_6$ (=Cr/2). Terms such as Al^{liq} refer to the cation fraction of $AlO_{1.5}$ in the liquid, Fm^{liq} is the sum $FeO^{liq} + MgO^{liq}$, and Mg'^{liq} is the cation fraction ratio $MgO^{liq}/(MgO^{liq} + FeO^{liq})$. Errors are similar to earlier models that utilize basalt compositions only. For the barometer, R^2 = 0.97 and the standard error of estimate (SEE) is 1.7 kbar for the regression data; for the thermometer R^2 = 0.96 and the SEE is 33 K. The models are applied to Neogene lavas from the Tibetan Plateau, and Neogene-Quternary lavas from the eastern Snake River Plain (SRP), Idaho. Crystallization depths for Tibet cluster at the middle/lower crust boundary. Magma-crust density relationships suggest that the middle crust may act as a level of neutral buoyancy. In the SRP, however, magmas appear to bypass several possible density traps. We suggest that fracture properties, such as dike size and aspect ratio, control magma transport in the SRP.

OVERVIEW

Numerous models have been proposed to explain the formation of magma chambers. Hypotheses fall roughly into two categories. In the first one, principles of fracture mechanics, states of stress, or mechanical properties of the lithosphere are invoked as controlling factors (e.g., Shaw 1980; Gudmundsson 1986; ten Brink and Brocher 1987; Kuntz 1992; Dvorak and Dzurisin 1993; Parsons and Thompson 1993; Putirka 1997). In the second model, density contrasts at various depths within the crust or lithosphere are emphasized (e.g., Stolper and Walker 1980; Ryan 1987; Hooft and Detrick 1993; Yang et al. 1999; Hansteen et al. 1998; Hermann et al. 2001). Although geophysical studies have demonstrated the existence of shallow-level magma chambers (e.g., Dvorak et al. 1983; Navin et al. 1998), they do not allow a resolution between these hypotheses. To understand why magmas stagnate, we need to determine the depths at which magma chambers form.

Crystallization depths are also relevant to understanding liquid evolution. It has long been suspected, from phenocryst relationships, that intermediate-SiO_2 lavas are produced through the interaction of basaltic magmas with high-SiO_2 partial melts

* E-mail: kputirka@csufresno.edu

of the crust (MacDonald and Katsura 1965; Eichelberger 1975). Later geochemical studies have demonstrated the importance of partial crystallization and consequent wall-rock assimilation (Hildreth and Moorbath 1988; Grove et al. 1988). But numerous questions remain. At what depths do crystallization, assimilation, and magma mixing take place? When primitive magmas are erupted, have they simply bypassed magma staging areas, or did they pond at greater (or shallower) depths prior to eruption? Finally, how does magma processing relate to tectonics. For example, the transition from intermediate to bi-modal (basalt + rhyolite) style volcanism in such areas as the Basin and Range Province has been linked to tectonic rates of extension (e.g., Gans et al. 1989). But what are the precise controls on these links?

TESTS OF EXISTING CRYSTALLIZATION BAROMETERS, AND RELATED MODELS

Igneous thermobarometers can be used to provide important clues to problems of magma transport because transport models make clear predictions about the depths at which magma chambers form. One promising method for depth estimation involves the use of temperature- and pressure-sensitive mineral-melt equilibria (Nielsen and Drake 1979; Nimis 1995, 1999; Putirka et al. 1996), which have been employed to address magma transport issues on basaltic samples (e.g., Putirka 1997; Yang et al. 1999). But it is unclear whether such models can be applied to more evolved lava compositions, or liquids that are nominally hydrous. We test several existing methods of pressure estimation using experiments conducted on hydrous compositions from Sisson and Grove (1993a, 1993b), Gaetani and Grove (1998), and Müntener et al. (2001), and SiO_2-rich compositions from Esperança and Holloway (1986) and from this study (Tables 1–3).

When the models of Putirka et al. (1996) are applied to hydrous and high-SiO_2 compositions, the models underestimate crystallization pressures (Fig. 1a). The models of Nimis and Ulmer (1998) fare little better with such compositions (Fig. 1b) [despite their use of some hydrous compositions, the models of Nimis (1999) are slightly worse]. These targeted methods of *P* estimations thus require improvement.

A slightly different tactic for pressure estimation involves use of the MELTS and pMELTS models of Ghiorso et al. (2002) and Ghiorso and Sack (1995). Although MELTS and pMELTS are not calibrated as barometers or thermometers (and to our knowledge are not claimed to be used as such by their authors), it is not uncommon for these models to be used to estimate crystallization conditions for natural samples (e.g., Salvioli et al. 2002; Trua et al. 2002; Guetschow and Nelson 2002; Kolsrud et al. 2001; Kilinc et al. 1999). In the MELTS/pMELTS models, pressure is not computed directly from compositional input, but instead, phase compositions are calculated for a given bulk composition using *P* and *T* as input; in practice calculated phase compositions are then compared to observed rock and/or phenocryst compositions. In contrast to the models of Putirka et. al. (1996) and Nimis and Ulmer (1998), the MELTS and pMELTS calibrations utilize a much wider range of liquid compositions, and the Gaetani and Grove (1998) and Sisson and Grove (1993a, 1993b) experiments are part of their calibration database. Given that their calibration data encompass hydrous compositions and liquids with >75 wt% SiO_2, (see Fig. 2 in Ghiorso et al. 2002), do these models provide a better, more versatile method of estimating crystallization conditions or phase compositions?

Because the clinopyroxene component jadeite (Jd; $NaAlSi_2O_6$) is crucial to pressure, we used MELTS and pMELTS to recover this clinopyroxene component from experimental data. Because coexisting liquid compositions are also critical to estimating crystallization pressures, we also tested calculated values for the mole fraction ratio:

TABLE 2. Experimental conditions

Expt. no.	*P* (kb)	*T* (C)	Run time (days)	Starting composition
G185-4-TE	10	1050	4.8	G185
G185P-1	15	1100	3.8	G185 + Phlogopite
G185-2-TE	20	1200	3	G185
G185-3-TE	30	1300	3	G185
G200-1-TE	10	1100	3.7	G200
G200-5-TE	10	1125	2.6	G200
G200-2-TE	20	1200	3.7	G200
G200-3-TE	35	1300	3	G200
KH1-2	10	850	1.2	KH1
KH1-4	10	850	1.9	KH1
KH1-5	10	1100	1.75	KH1
KH1-3	15	900	1	KH1
KH1-8-TE	15	1000	2.7	KH1 + H_2O
KH1-6	20	1200	2.7	KH1
KH1-9-TE	20	1250	2.3	KH1 + H_2O
MH7-2-TE	10	1050	10	MH7 + H_2O
MH7-3	20	1100	10	MH7 + H_2O
MH7-7TE	20	1250	1.7	MH7 + H_2O
MH8-13-TE	10	1100	2	MH8
MH8-9-TE	15	1100	1.7	MH8
MH8-8	20	1200	2.7	MH8
MH8-15-TE	20	1250	0.7	MH8 + H_2O
NE-4	10	1000	2.1	F17 + Phlogopite
F17-1	20	1100	2	F17 + Phlogopite
LPNE-5	10	1150	0.5-1 (*)	TK-17-5 + Phlogopite
TK17-5-2-TE	15	1200	0.75	TK-17-5 + H_2O

* Quench caused by power failure.

TABLE 1. Starting compositions

	SiO_2	TiO_2	Al_2O_3	Fe_2O_3	FeO	MnO	MgO	CaO	Na_2O	K_2O	Cr_2O_3	P_2O_5	F	Total
G185	51.4	1.85	14.62	3.35	3.02	0.14	4.03	7.59	4.60	4.77	0.09	1.85	–	97.3
G200	56.7	1.43	13.80	2.93	2.64	0.10	4.37	6.35	4.02	5.40	0.08	–	–	97.8
KH1	65.3	0.76	15.16	4.94	–	0.08	2.20	4.32	3.62	3.22	–	0.18	–	99.8
MH7	56.5	1.55	15.35	8.68	–	0.14	4.82	6.64	3.92	1.18	–	0.29	–	99.1
MH8	52.7	1.75	16.05	10.7	–	0.16	5.53	8.19	3.78	1.15	–	0.32	–	100.3
TK-17-5	49.8	1.38	15.92	–	9.38	0.18	8.88	11.28	3.00	0.11	0.00	–	–	99.9
F1-17	38.8	3.62	14.44	7.51	6.37	0.24	4.58	11.99	4.94	4.63	2.01	–	–	99.1
Phlogopite	40.7	0.00	14.90	–	3.17	0.00	25.26	0.00	0.26	9.71	0.00	–	5.27	99.2

Note: KH and MH prefixes indicates samples from Kramer Hills, CA and Muroc Hills, CA; GXXX prefixes denote Shoshonites from Tibet (Arnaud et al. 1992).

TABLE 3. Experimental clinopyroxene and glass compositions in wt%

Run no.	*T*(C)	*P*(kb)	phase	SiO_2	TiO_2	Al_2O_3	FeO	MnO	MgO	CaO	Na_2O	K_2O	Cr_2O_3	total
G185P-1	1100	15	cpx	50.3(6)	0.8(3)	6.3(3)	9.8(2)	0.28(2)	14.6(3)	15.7(5)	1.1(1)	0	0.33(4)	99.2
			glass	55.9(8)	1.29(4)	17.89(3)	6.8(2)	0.12(1)	3.11(7)	4.16(8)	1.4(4)	3.4(8)	0	94.1
G185-2-TE	1200	20	cpx	50.2(6)	1.1(1)	9.2(6)	8.8(5)	0.19(2)	10.9(4)	16.8(5)	2.0(1)	0	0	99.2
			glass	52.6(9)	2.15(7)	15.7(2)	7.6(4)	0.11(2)	2.6(2)	5.1(3)	1.4(2)	3.6(5)	0	90.9
G185-3-TE	1300	30	cpx	50.6(2)	0.80(6)	9.5(6)	8.08(7)	0.19(2)	11.0(5)	17.1(5)	2.1(2)	0	0.01	99.4
			glass	51.3(9)	2.2(1)	15.2(4)	7.1(7)	0.13(2)	3.8(5)	5.1(1.0)	1.7(2)	4.0(6)	0	90.5
G200-1-TE	1100	10	cpx	53.2(8)	0.59(6)	1.8(6)	6.7(3)	0.22(3)	16.5(4)	19.9(8)	0.6(1)	0.01(1)	0	99.5
			glass	60.1(9)	1.0(2)	18.4(4)	4.1(2)	0.08(2)	0.61(4)	1.70(6)	4.6(2)	4.9(2)	0	95.5
G200-5-TE	1125	10	cpx	52.7(4)	0.6(1)	1.5(2)	7.4(3)	0.34(4)	16.6(3)	20.0(3)	0.54(6)	0	0	99.7
			glass	64.2(9)	1.5(5)	18.8(4)	3.0(1.2)	0.05(2)	0.8(4)	1.7(2)	2.4(8)	4.3(8)	0	96.8
G200-2-TE	1200	20	cpx	52.2(6)	0.7(2)	7.2(1.0)	8.3(3)	0.22(2)	12.1(4)	16.2(8)	2.3(2)	0	0.29	99.4
			glass	61.0(4)	1.48(4)	16.3(2)	4.8(2)	0.09(2)	2.00(5)	2.96(8)	1.09(7)	3.4(5)	0	93.1
G200-3-TE	1300	35	cpx	53.5(5)	0.21(2)	5.2(3)	4.9(2)	0.06(2)	15.2(3)	18.3(5)	1.69(6)	0	0	99.1
			glass	58.5(5)	1.2(2)	15.5(5)	5.0(9)	0.02(1)	2.8(4)	4.0(7)	1.5(4)	3.9(9)	0	92.4
KH1-2	850	10	cpx	50.8(5)	0.7(1)	4.2(6)	8.5(5)	0.23(2)	15.0(7)	19.0(6)	0.46(2)	0	0.3	99.2
			glass	71.3	0.05	15.1	2.59	0.13	0.93	2.18	2.64	2.95	0	97.9
KH1-4	850	10	cpx	51.2(4)	0.5(1)	3.4(2)	8.2(5)	0.24(5)	15.1(6)	19.5(2)	0.45(4)	0	0.02	98.6
			glass	68.9(9)	0	16.1(3)	1.46(1)	0.03(1)	0.40(3)	1.72(4)	0.21(8)	0.7(3)	0	89.5
KH1-5	1100	10	cpx	50.45(3)	0.58(8)	3.5(4)	10.7(4)	0.33(3)	13.8(2)	19.2(3)	0.40(2)	0	0.03(1)	99
			glass	69.4(7)	0.66(2)	15.7(2)	4.1(1)	0.08(1)	1.26(3)	3.11(3)	0.6(2)	2.7(7)	0	97.6
KH1-3	900	15	cpx	50.9(2)	0.43(2)	3.5(1)	9.0(2)	0.38(1)	14.2(4)	19.2(2)	1.3(3)	0	0.03(3)	98.9
			glass	60.5(9)	0.31(2)	15.6(6)	1.7(4)	0.15(1)	0.8(1)	1.78(9)	1.9(3)	1.1(1)	0	83.8
KH1-8-TE	1000	15	cpx	50.2(9)	0.7(2)	4.6(6)	9.9(8)	0.35(2)	14.7(1.2)	18.8(2)	0.31(1)	0	0	99.6
			glass	66.1(1.1)	0.47(3)	16.3(4)	2.91(8)	0.14(1)	0.94(3)	2.37(5)	0.4(1)	2.1(2)	0	91.7
KH1-6	1200	20	cpx	49.9(4)	0.74(7)	10.0(9)	9.6(1.0)	0.22(4)	10.5(6)	16.3(6)	2.0(3)	0	0	99.3
			glass	70.9(1.1)	0.61(2)	15.5(4)	2.9(1)	0.06(2)	1.0(4)	2.80(8)	0.6(2)	2.2(5)	0	96.6
KH1-9-TE	1250	20	cpx	53.2(2)	0.11(2)	6.43(9)	7.6(2)	0.31(1)	14.5(4)	15.8(3)	0.994(5)	0	0.34(2)	99.3
			glass	65.4(7)	0.60(2)	15.9(2)	4.5(2)	0.184(4)	2.41(6)	4.17(6)	1.2(5)	2.4(6)	0	96.8
MH7-2-TE	1050	10	cpx	49.9	0.29	6.52	11.76	0.04	14	15.78	0.97	0	0	99.3
			glass	55.2	1.68	16.7	5.98	0.08	1.47	4.33	4.45	2.26	0.02	92.2
MH7-3	1100	20	cpx	51	1.05	4.05	8.63	0.34	13.78	19.1	0.59	0	0.56	99.1
			glass	70.2(5)	0.84(2)	15.8(1)	2.17(7)	0.12(1)	0.72(5)	2.1(1)	0.45(2)	1.25(2)	0	93.7
MH7-7TE	1250	20	cpx	52.3(7)	0.334(2)	7.4(2)	8.7(2)	0.23(2)	14.9(4)	13.6(5)	1.70(7)	0	0.02(1)	99.2
			glass	57.4(8)	1.66(1)	16.2(2)	7.8(2)	0.14(2)	4.39(1)	5.60(8)	0.3(2)	0.8(4)	0	94.3
MH8-13-TE	1100	10	cpx	50.3(4)	0.79(5)	6.8(4)	9.88(6)	0.25(1)	14.4(3)	16.3(3)	0.70(1)	0	0	99.4
			glass	53.9(6)	1.72(4)	17.4(3)	9.4(1)	0.17(2)	4.2(1)	6.5(1)	0.9(3)	1.1(1)	0	95.3
MH8-9-TE	1100	15	cpx	50.2(3)	0.89(3)	6.7(1)	13.2(4)	0.39(3)	13.3(2)	14.2(2)	0.69(3)	0	0	99.6
			glass	60.4(6)	1.68(4)	18.5(2)	6.7(2)	0.18(2)	2.07(4)	4.10(5)	0.2(2)	0.6(4)	0	94.4
MH8-8	1200	20	cpx	50.2(1)	1.18(5)	9.2(1)	10.7(2)	0.34(1)	11.4(1)	15.3(4)	1.37(1)	0	0	99.7
			glass	62.8(7)	1.80(4)	17.1(2)	5.4(2)	0.18(1)	1.74(3)	4.19(5)	0.5(5)	1.5(5)	0	95.2
MH8-15-TE	1250	20	cpx	51.0(3)	0.68(3)	10.8(4)	8.1(3)	0.16(2)	10.8(3)	15.1(3)	2.6(1)	0	0	99.2
			glass	59.2(1.0)	2.23(4)	17.6(3)	8.1(2)	0.10(1)	2.1(1)	4.0(1)	0.09(4)	0.09(8)	0	94.3
NE-4	1000	10	cpx	47.5(1.2)	1.8(4)	5.7(1.8)	13.3(1.0)	0.34(4)	8.1(1.4)	22.0(8)	0.9(2)	0	0	99.6
			glass	51.2(9)	0.74(7)	20.3(4)	9.0(3)	0.25(2)	0.58(9)	4.3(3)	2.1(2)	6.2(7)	0	94.7
F17-1	1100	20	cpx	45.1(1.5)	2.3(5)	13.8(1.5)	10.1(7)	0.22(3)	6.3(6)	18.2(8)	3.1(2)	0	0.31(0)	99.4
			glass	47.5(9)	1.52(6)	20.4(5)	10.2(5)	0.25(2)	1.3(1)	3.8(3)	2.3(3)	6.2(8)	0	93.5
LPNE-5	1150	10	cpx	50.7(7)	0.7(2)	6.7(1.0)	6.1(6)	0.12(2)	17.3(4)	17.1(9)	0.49(3)	0	0	99.5
			glass	48.0(6)	1.32(3)	17.6(2)	7.5(2)	0.082(1)	6.4(1)	10.0(2)	1.9(1)	1.48(2)	0	94.3
TK17-5-2-TE	1200	15	cpx	50.6(3)	0.44(6)	7.3(5)	5.3(2)	0.16(1)	15.4(3)	19.1(5)	0.89(6)	0	0	99.2
			glass	44.3(3)	1.99(3)	17.0(2)	9.4(2)	0.21(1)	6.8(2)	7.0(1)	0.6(1)	0.04(1)	0	87.3

Note: cpx = clinopyroxene

$$\frac{Jd^{cpx}}{NaO_{0.5}^{liq}AlO_{1.5}^{liq}(SiO_2^{liq})^2} = K(Jd-liq)$$

(see Eq. 1 below). MELTS and pMELTS do not perform well for Jd; even for their calibration data, Jd contents are systematically overestimated (Fig. 1c). MELTS and pMELTS also yield unsatisfactory results for other phase components. For example, although MELTS and pMELTS yield a reasonably good fit to predicted vs. measured values for SiO_2 in experimental liquids (R^2 = 0.69), other liquid components such as Na_2O^{liq} (R^2 = 0.19) or $Al_2O_3^{liq}$ (R^2 = 0.23), or pyroxene components such as diopside + hedenbergite (R^2 = 0.31) are recovered poorly (see also Putirka 1999). Such errors combine to yield very unsatisfying results for K(Jd – liq) (Fig. 1d). The magnitude of these errors, when input into existing thermobarometers, result in an uncertainty in P exceeding 9 kbar. We thus cannot recommend use of MELTS or pMELTS to calculate crystallization conditions, or phase composition, and would not suggest that these models be used to test for mineral-melt equilibrium.

Consequently, there is a critical need for models that are specifically calibrated to the task of P and T estimation, and that can be applied to evolved liquids and nominally hydrous systems. To rectify the lack of a practical set of thermobarometers that can be applied to such systems, new thermobarometers have been calibrated based on new experiments. The calibration data encompass experimental liquid compositions that are volatile-bearing and that range to 71.3 wt% SiO_2.

METHODS

As with prior calibrations (Putirka et al. 1996), the new models are based on regression analysis of partial-melting experiments where clinopyroxenes are grown at a range of pressures and temperatures, from a range of liquid compositions. For a barometer, we use the equilibrium constant (K_{eq}) for the jadeite

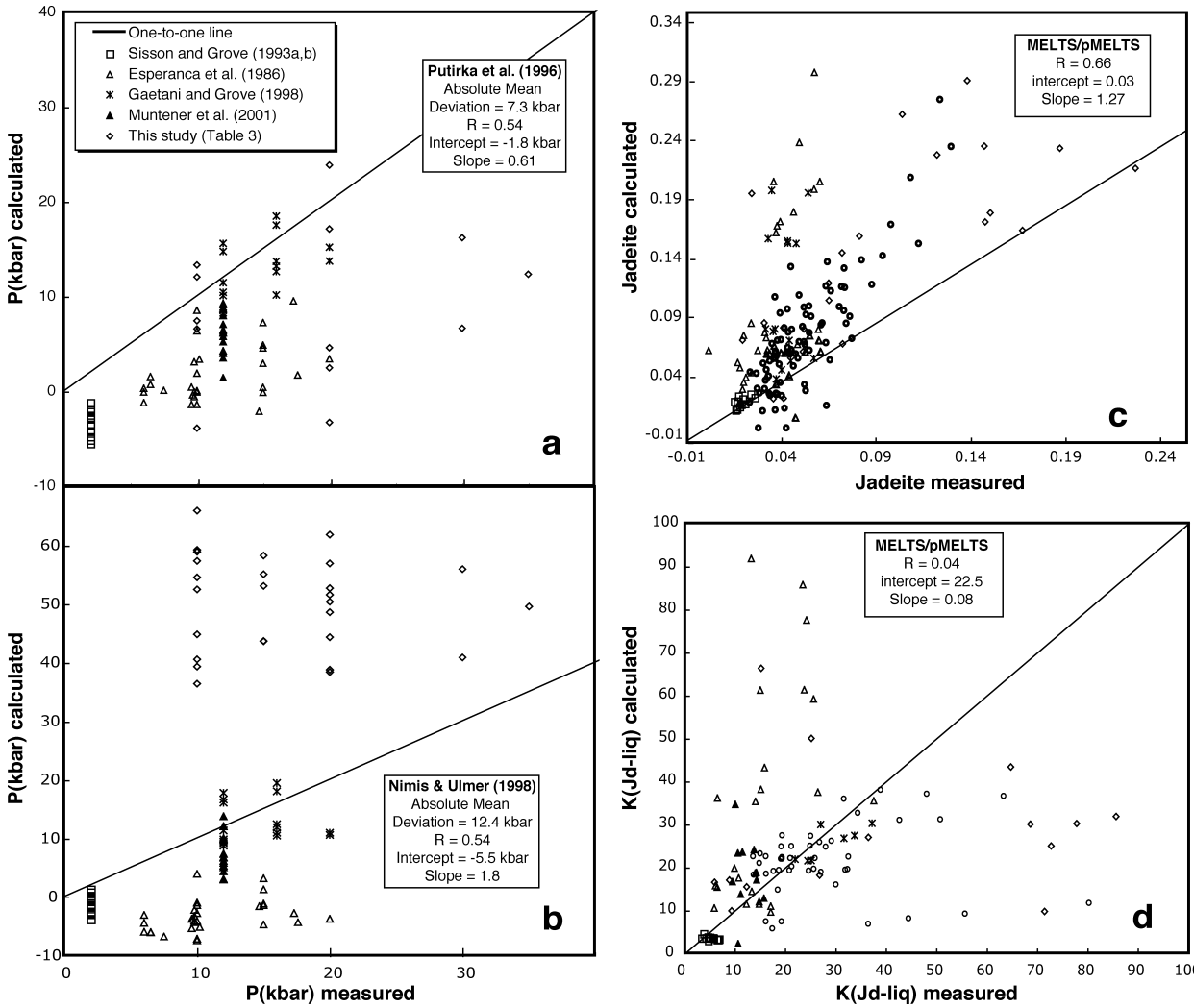

FIGURE 1. (**a**) Thermobarometers from Putirka et al. (1996; models P1 and T2) were used to predict pressures for hydrous and high-SiO_2 experimental compositions. Calculated pressures are systematically low for most experiments, indicating that the models of Putirka et al. (1996) cannot be extrapolated to high-SiO_2 lava compositions. (**b**) The Nimis and Ulmer (1998) model was used to predict pressures for these same hydrous and high-SiO_2 experimental data [models of Nimis (1999) yield a poorer fit]. (**c**) and (**d**) The MELTS [for $P < 10$ kbar; Ghiorso and Sack (1995)] and pMELTS [for $10 < P < 20$ kbar; Ghiorso et al. (2002)] models were used to recover values for Jd and K(Jd-liq) for experimental data. In (**c**) Jd is calculated based on the pyroxene component algorithm described in the Methods section, using observed experimental clinopyroxene compositions, and calculated clinopyroxene compositions from MELTS and pMELTS. In **d**, the mole fraction ratio describing Jd crystallization, K(Jd – liq) (see text) is calculated using observed experimental liquid and clinopyroxene compositions, and calculated liquid and clinopyroxene compositions from MELTS/pMELTS. Combined compositional error from MELTS/pMELTS translates to a P uncertainty exceeding 9 kbar. Open circles in (**c**) and (**d**) are experiments on basaltic compositions from Putirka et al. (1996), Robinson et al. (1998), and Bartels et al. (1991) that were used in the calibration of pMELTS. R = correlation coefficient. Slopes and intercepts of regressions through calculated vs. measured values are indicated, as are the mean of absolute values for P (calculated) – P (measured).

crystallization equilibrium:

$$NaO_{0.5}^{liq} + AlO_{1.5}^{liq} + 2SiO_2^{liq} = NaAlSi_2O_6^{cpx}. \quad (1)$$

The molar volume change of Equation 1 at 1 bar is 23.5 cm^3/mol [based on partial molar volume data from Lange and Carmichael (1987) and Robie et al. (1979)], making it perhaps the most P-sensitive igneous equilibrium involving major-element components of a common silicate phase. Equation 1 thus represents one of our best opportunities to estimate crystallization pressures using a commonly encountered mineral, and that involves components that are easily measured with the electron microprobe. The entropy change of Equation 1 is non-zero (Richet et al. 1993), which means the equilibrium also has a temperature dependence. We therefore need a clinopyroxene thermometer, for which we use the K_{eq} for the jadeite (Jd) – diopside (Di) + hedenbergite (Hd) exchange: equilibrium,

$$CaFmSi_2O_6^{cpx} + NaO_{0.5}^{liq} + AlO_{1.5}^{liq} = NaAlSi_2O_6^{cpx} + CaO^{liq} + FmO^{liq}, \quad (2)$$

where Fm = FeO + MgO, and $CaFmSi_2O_6$ represents $Ca(Fe,Mg)Si_2O_6$, or DiHd.

Component calculation procedures

Liquid components are treated as cation fractions of the oxides SiO_2, TiO_2, $AlO_{1.5}$, FeO, MnO, MgO, CaO, $NaO_{0.5}$, $KO_{0.5}$ and $CrO_{1.5}$. (The wt% of oxides such as Al_2O_3, which have more than one cation per formula unit, are divided by the molecular weight of the single cation unit, i.e., 50.981 for $AlO_{1.5}$). H_2O was not included in the calculation of liquid cation fractions because many experi-

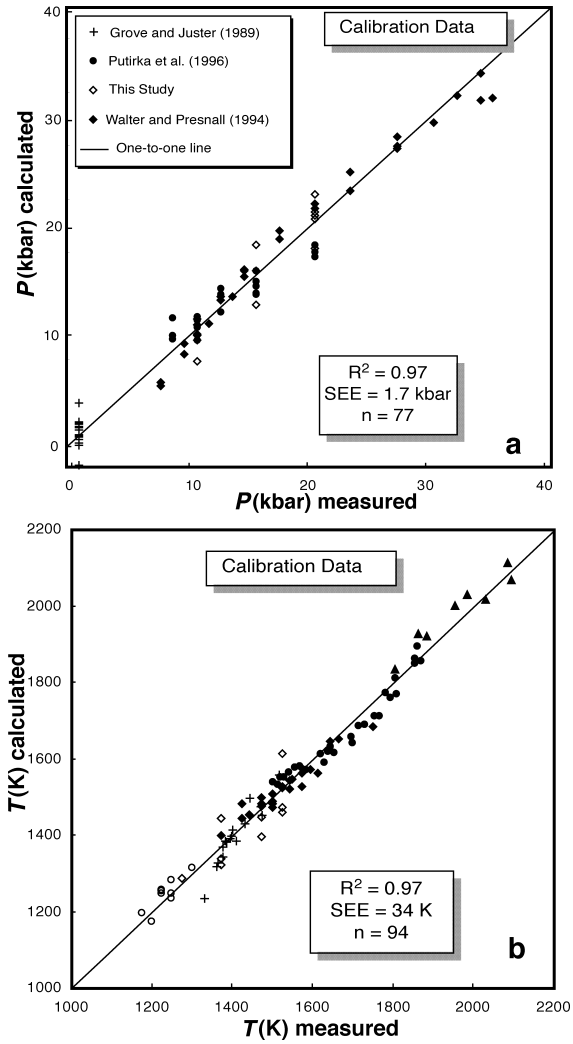

ments in both the test and regression data sets were not analyzed for H_2O. Oxide percentages were not renormalized to 100 prior to the calculation of cation fractions, as this step did not appear to lead to any improvement in model precision.

Clinopyroxene formulae were calculated following a scheme that is similar to Lindsley (1983). We began with clinopyroxene cations calculated on the basis of six O atoms (see Klein 2001, table 3.17), and $^{IV}Al = 2 - Si$; ($^{VI}Al = Al - {}^{IV}Al$); we examine the quality of analyses by checking that cations sum to 4. The calculations procedure used in this study is as follows:

1. Jd = ^{VI}Al or Na, whichever is less.
2. If excess ^{VI}Al exists after forming Jd, CaTs ($Ca^{IV}Al^{VI}AlSiO_6$) = ^{VI}Al – Jd.
3. If ^{IV}Al > CaTs, CaTi ($CaTiAl_2O_6$) = [^{IV}Al – CaTs]/2.
4. CrCaTs ($CaCr_2SiO_6$) = Cr/2.
5. DiHd ($CaFmSi_2O_6$) = Ca – CaTi – CaTs – CrCaTs.

6a. EnFs ($Fm_2Si_2O_6$) = [Fm – DiHd]/2.

Or, for Ca-poor pyroxenes:

6b. If there is a Ca deficiency after forming either CaTs or CaTi, then DiHd (and possibly CaTs) is set to zero, and the following components are formed:
(a) CaTs = Ca.
(b) Any remaining ^{VI}Al ($^{VI}Al_{ex} = {}^{VI}Al - CaTs$) is used to form FmCaTs ($Fm^{IV}Al^{VI}AlSiO_6$) = $^{VI}Al_{ex}$ – CaTs.
(c) FmTi ($FmTi^{IV}Al^{VI}AlO_6$) = [^{IV}Al – CaTs – FmCaTs]/2.
(d) EnFs = [Fm – FmCaTs – FmTi]/2.

In the above notation, DiHd represents diopside + hedenbergite, EnFs = enstatite + ferrosilite, CaTs is the Ca-Tschermak's component, and Jd is jadeite. The above algorithm is identical to that used by Putirka (1999), and differs from Putirka et al. (1996) only in that the Ca used to form CrCaTs is subtracted from DiHd above. In general, the CrCaTs component is small in the experimental data set, so systematic error obtained by ignoring CrCaTs will be small. Note that only steps 1–5 are needed to use models A and B of Table 4. Additional components are used for the saturation surface models of Putirka (1999). By

◀

FIGURE 2. (**a**) Model A of Table 4 was used to recover pressures for the calibration data set. (**b**) Model (B) was used to recover temperatures for the calibration data. As a sample calculation, models A and B solved simultaneously for sample KH1-4 yield $P = 9.34$ kbar, $T = 1219.6$ K. See text for discussion of regression data.

TABLE 4. New igneous thermobarometers and Fe-Mg exchange constants

Equation	Model
$P(\text{kbar}) = -88.3 + 2.82\times10^{-3}T(\text{K})\ln\left[\frac{[Jd^{cpx}]}{\left[Na^{liq}Al^{liq}\left(Si^{liq}\right)^2\right]}\right] + 2.19\times10^{-2}T(K) - 25.1\ln[Ca^{liq}Si^{liq}] + 7.03[Mg'^{liq}] + 12.4\ln[Ca^{liq}]$	(A)
$\frac{10^4}{T(\text{K})} = 4.60 - 4.37\times10^{-1}\ln\left[\frac{[Jd^{cpx}Ca^{liq}Fm^{liq}]}{[DiHd^{cpx}Na^{liq}Al^{liq}]}\right] - 6.54\times10^{-1}\ln[Mg'^{liq}] - 3.26\times10^{-1}\ln[Na^{liq}] - 6.32\times10^{-3}[P(\text{kbar})] - 0.92\ln[Si^{liq}] + 2.74\times10^{-1}\ln[Jd^{cpx}]$	(B)
$\ln\left(\frac{Mg^{liq}Fe^{cpx}}{Mg^{cpx}Fe^{liq}}\right) = 4.05\times10^{-2} - \frac{2.01\times10^3}{T(\text{K})}$	(C)
$\frac{Mg^{liq}Fe^{cpx}}{Mg^{cpx}Fe^{liq}} = 0.275 \pm 0.067$	(D)

Note: T is in Kelvins and P is in kbars. Clinopyroxene cations are calculated on the basis of 6 oxygens (Klein 2001). $DiHd^{cpx}$ is the fraction of diopside + hedenbergite in clinopyroxene, calculated as the fraction of Ca remaining after forming CaTs (= Al^{VI} – Jd), $CaTiAl_2O_6$ (=[Al^{IV} – CaTs]/2) and $CaCr_2SiO_6$ (= Cr/2). Jd^{cpx}, is the jadeite component, taken as the lesser of Na or Al^{VI}. The symbol Fm refers to total (FeO + MgO). Terms such as Ca^{liq} refer to the cation fraction of the indicated element in the liquid, and Ca^iSi^i the product of liquid cation fractions; $Mg'^{liq} = Mg^{liq}/(Mg^{liq} + Fe^{liq})$. See text for additional component calculation procedures.

adopting the above scheme, *P-T* estimates and the clinopyroxene saturation models of Putirka (1999) can be used with the same set of components. As an example of the calculation, the clinopyroxene of sample KH1-4 (Table 3) has the following components: Jd = 0.033, DiHd = 0.724; EnFs = 0.180; CaTs = 0.036; CrCaTs = 3.20×10^{-4}, and CaTi = 0.022.

As in Putirka et al. (1996), we do not calculate the acmite ($NaFe^{3+}Si_2O_6$) component of our clinopyroxenes, due to the inherent uncertainty in the calculation of Fe^{3+} (Lindsley 1983; McGuire et al. 1989). Charge-balance calculations (used to estimate Fe^{3+}) are nonetheless commonly used as a rough check for clinopyroxene stoichiometry, and we used the charge balance relationship of Lindsley (1983): $Fe^{3+} = Na + {}^{IV}Al - {}^{VI}Al - 2(Ti) - Cr$. For clinopyroxenes equilibrated in graphite capsules (which is the case for the high-pressure experiments in our calibration data sets) Fe^{3+} is expected, and calculated, to be very low. McGuire et al. (1989) showed that such calculations do not guarantee that the Fe^{3+} content of such minerals will be low. As an indirect check, we used the expressions of Holloway et al. (1992) to estimate Fe^{3+}/Fe^{total} for our liquid compositions. In the presence of graphite, the highest attainable f_{O_2} values would be achieved at CO_2 vapor saturation, in which case Fe^{3+}/Fe^{total} in our experiments reach a maximum value of 5.6% (Holloway et al. 1992; solubility calculations suggest that our experiments would reach saturation at an average of 1.2 wt% CO_2, with a range of 0.8 to 2.7 wt%). Because our experiments appear not to be vapor saturated, f_{O_2} and Fe^{3+}/Fe^{total} values are likely to be lower. Indeed, Holloway et al. (1992) noted that in unsealed graphite capsules, loss of CO_2 can lead to very low Fe^{3+}/Fe^{total} (though, because our experiments were performed using $BaCO_3$ pressure media, CO_2 loss may actually be minimal). Although our experiments are expected to have low Fe^{3+}/Fe^{total} values, the 1 atm experiments used for calibration of the barometers (see below) were run as high as 2.9 log units above the quartz-fayalite-magnetite buffer, and hence our total calibration data set encompasses a very wide range of f_{O_2} conditions. Significantly, error on pressure estimates is uncorrelated with experimental f_{O_2} for the 1 atm experiments ($R^2 = 0.098$). This result suggests that there should be no systematic error with regard to f_{O_2}, and that our models and component calculation schemes should apply to rocks equilibrated at a wide range of f_{O_2} conditions.

Thermodynamic models

The approach to calibration is semi-theoretical. The thermbarometers are based on thermodynamic relationships, but empirical parameters are added when needed to improve model precision. To obtain the form of the thermobarometers, we expand the familiar expression:

$$-\mathrm{R}T\ln K_{\mathrm{eq}} = \Delta G_r^0 \tag{3}$$

to obtain the relationship:

$$\ln K_{\mathrm{eq}} = -\frac{\Delta H_r^0}{\mathrm{R}T} + \frac{\Delta S_r^0}{R} - \frac{(P - P_{\mathrm{o}})\Delta V_r^0}{\mathrm{R}T}. \tag{4}$$

In Equations 3 and 4, K_{eq} represents the equilibrium constant for a given equilibrium, R is the gas constant, T is temperature, P is pressure, and P_o is a reference pressure. ΔG_r^0 is the standard-state Gibbs free energy change for a given equilibrium, and ΔH_r^0, ΔS_r^0, and ΔV_r^0, are the enthalpy, entropy and volume differences (products – reactants) of the equilibrium at P_o (usually 1 bar) and a reference temperature (usually 298 K). For purposes of regression, it is essential to isolate the variables of interest (Putirka 1999), which in this case are T and P. Equation 3 can be rearranged algebraically so that P appears as a dependent variable:

$$P(\mathrm{kb}) = -\frac{\mathrm{R}T\ln K_{\mathrm{eq}}}{\Delta V_r^0} + \frac{T\Delta S_r^0}{\Delta V_r^0} - \frac{\Delta H_r^0}{\Delta V_r^0}. \tag{5}$$

Equation 4 also can be arranged to isolate T as a variable:

$$\frac{1}{T} = -\frac{R\ln K_{\mathrm{eq}}}{\Delta H_r^0 + P\Delta V_r^0} + \frac{\Delta S_r^0}{\Delta H_r^0 + P\Delta V_r^0}. \tag{6}$$

In Equation 6, the quantities P and K_{eq} are not algebraically separable. To perform a linear regression analysis, we sacrifice the thermodynamic form of Equation 6 and add P as an empirical parameter:

$$\frac{1}{T} = -\frac{R\ln K_{\mathrm{eq}}}{\Delta H_r^0} + \frac{\Delta S_r^0}{\Delta H_r^0 + P\Delta V_r^0} + A * P, \tag{7}$$

where A is a regression coefficient with no ostensible thermodynamic significance.

To obtain Equation 4 from 3, the assumption is made that ΔH_r^0, ΔS_r^0, and ΔV_r^0 are approximately constant over the *P-T* range of interest. For the case of ΔH_r^0 and ΔS_r^0, this assumption is tantamount to assuming that the heat capacity difference between products and reactants is negligible ($\Delta C_P = 0$). Where such assumptions do not hold, Equation 3 can instead be integrated assuming ΔC_P = a constant, or $\Delta C_P = f(T)$. Similarly, one can account for variations in molar volume changes: $\Delta V_r = f(T,P)$. Such equations were developed in Putirka (1998), and were explored as possible models in the present study.

Equilibrium constants for Equations 1 and 2 are written assuming ideal behavior ($a_i = X_i$). The liquid and mineral components that appear in these expressions, however, are known to be non-ideal, so this strategy assuredly introduces some error. Such an error can be accounted for through the addition of compositional parameters to the regression equations. These parameters, though perhaps empirical, are not entirely lacking in thermodynamic significance. Separation of ideal and non-ideal quantities is possible due to the logarithmic relationships of expressions involving K_{eq}, and if written in logarithmic form, it is possible to relate such compositional corrections directly to activity coefficients (Putirka et al. 1996; Putirka 1999). This strategy offers an advantage with regard to numerical analysis in that non-linear regression techniques are avoided (see Putirka 1999). Nevertheless, activity modeling is not our goal, and regression strategies were selected so as to yield the highest level of precision for estimates of P and T.

Experimental and analytical methods

The experimental assemblies and analytical methods utilized are identical to those outlined in Putirka et al. (1996), and are briefly reviewed here. Experiments were performed at the Lawrence Livermore National Laboratory (LLNL), using Boyd-England piston-cylinder presses with 1/2 inch bore diameters, $BaCO_3$ pressure media, and Pb-foil sleeves. Pressure was applied using the cold-piston-in technique with friction corrections for $BaCO_3$ (Fram and Longhi 1992). Temperatures were measured using type-D thermocouples (W + 3%Re/W + 25%Re); no pressure correction was applied to thermocouple emf. Run times varied between 2 and 10 days; in most cases, 1–3 days were sufficient to achieve homogeneous glass and mineral phases. In contrast to the bulk compositions employed by Putirka et al. (1996), the high-silica liquid compositions of this study posed no difficulty in recovery of glass. All runs were therefore quenched using the usual "thermal quench" procedure, in which power is shut off at the end of an experimental run while the experimental run is at target pressure. Percent crystallinity for our experiments ranges from 5–55%.

Experimental starting compositions (Table 1) include andesites and dacites from the western Mojave Desert and shoshonites from the Tibetan Plateau (Table 1); clinopyroxenes were equilibrated with these bulk compositions at pressures of 10–35 kbar (Table 2). Glass compositions recovered from experiments on these compositions range up to 71.3 wt% SiO_2 (Table 3), significantly expanding upon the SiO_2 range explored by Putirka et al. (1996). Natural SiO_2-rich lava compositions generally contain non-trivial amounts of H_2O and/or CO_2, and we were interested in whether our thermobarometers might apply to such lavas. Some bulk compositions of prior studies were known to be nominally hydrous, and CO_2-bearing (e.g., ugandites from Putirka et al. 1996). To provide additional experimental tests, we added 1–2.5 µL H_2O to several of our experimental capsules, and phlogopite to several others (Table 2). We also tested whether our experiments would retain more water if sealed platinum outer capsules were used. Experience showed, however, that at least when $BaCO_3$ pressure media were used, volatile retention was no less for single graphite capsules than for double capsule assemblies.

In the present experiments, glasses contain up to 12.7 wt% volatiles (Table 3); vesicles are absent from all experiments, suggesting that our glasses may be volatile under-saturated. To check that inferred volatile contents are consistent with experimental constraints for water saturation, we utilized the models of Dixon et al. (1995) and Moore et al. (1998) to calculate water solubilities. For these calculations, we used both the modified Redlich-Kwong equation of state, with constants from Holloway (1977) and Halbach and Chaterjee (1982), to calculate the fugacity of H_2O. All variants of these models yielded water saturation levels that exceeded observed water contents for the data of Gaetani and Grove (1998) and Müntener et al. (2001), suggesting that these models can be extrapolated to elevated pressure. In all cases, calculated levels of water saturation exceeded inferred volatile contents for the experiments of this study; low glass totals are thus consistent with experimental constraints on water solubility. As additional evidence that these low totals reflect dissolved water, samples

KH-1, KH-3, F17-1, and G186-4 are biotite saturated, sample LPNE-1 is phlogopite saturated, and sample MH7-7 is hornblende saturated (no reaction rims on clinopyroxene were observed in any experiment; micas and hornblende are euhedral, entirely surrounded by glass). These new data thus represent a significant expansion over the volatile contents of Putirka et al. (1996), where inferred volatile contents ranged to 6.5 wt%. As our experiments were run in graphite capsules, there is also the possibility that our samples contain dissolved CO_2. Although we do not know the range of CO_2-H_2O concentrations, our calibration and test data sets clearly cover a wide range in these variables, and as noted above, saturation calculations suggest that up to 2.7 wt% CO_2 might be dissolved in our samples.

Although none of the clinopyroxenes exhibited visible zoning in back-scattered electron images, the reported clinopyroxene analyses represent rim compositions from minerals in contact with glass, as dictated by prior experience (see Putirka et al. 1996 for discussion of analytical strategies). Reported glass analyses similarly represent regions in proximity to clinopyroxene crystals. Glasses, however, appeared to be homogenous for all experiments reported in Tables 2 and 3. When analyses indicated that the glass was inhomogeneous, the experiment was either re-run using the same starting materials and target P and T, but with longer run times, or was discarded. (Attempts to equilibrate clinopyroxenes from high-silica obsidian starting materials were unsuccessful, even with two-week run times).

Mineral and glass analyses were performed using the JEOL 733 electron microprobe facilities at LLNL, and the Cameca SX50 electron microprobe at the University of Massachusetts, Amherst (UMA). The accelerating voltage in both cases was 15 kV. For mineral analyses at LLNL, a 1 μm diameter beam spot and a beam current of 20 nA were employed. To minimize volatile loss of alkalis, glasses were analyzed using a 10 μm beam spot and a 15 nA beam current. Some mineral grains that were large enough were also re-analyzed at UMA using a 10 μm beam spot and a 15 nA beam current; no discernible difference in clinopyroxene Na_2O (or other oxide) contents were apparent between analyses performed at UMA and LLNL. Standard deviations for repeated analyses of glass standard USNM 113716 are as follows: SiO_2 (0.47), TiO_2 (0.03), Al_2O_3 (0.19), FeO (0.12), MnO (0.02), MgO (0.09), CaO (0.06), Na_2O (0.08), K_2O (0.01), and Cr_2O_3 (0.01).

Data and regression strategies

The data used for calibration of the barometer (model A, Table 4, Fig. 2a) include: 1 atm data from Grove and Juster (1989); ugandite, Woodlark Basin, and Mid-Atlantic ridge compositions from Putirka et al. (1996); SCAM + Na data from Walter and Presnall (1994); and new experimental data (Table 3). The ankaramites of Putirka et al. (1996), shoshonites of this study (Gxxx prefix, Table 3) and samples KH1-2, KH1-8, KH1-9, KH1-12, and MH8-15 (Table 3) were reserved for use as test data. The thermometer (model B in Table 4, Fig. 2b) was calibrated using much of these same data. Sample WB-11 from Putirka et al. (1996), and several samples from Table 3 (KH1-2, KH1-3, KH1-4, MH8-13, F17-1, NE-4, TK17-5-2-TE, and LPNE-5) were reserved for use as test data for the thermometer. Data from Walter (1998) and Sen and Dunn (1994) also were added to the thermometer calibration data set. Additional data were collected from the literature for use as test data (Fig. 3). Of particular interest are test data from high-pressure experiments performed on K-latites (Esperança and Holoway 1986), hydrous basalts (Gaetani and Grove 1998), hydrous arc-related basalts and andesites (Baker and Eggler 1987), and hydrous arc-type lava compositions equilibrated at 1 and 2 kbar (Sisson and Grove 1993a, 1993b) and 12 kbar (Müntener et al. 2001). The calibration and test data encompass a very wide array of experimental arrangements and techniques, including samples run in unsealed and Pt-sealed graphite capsules, Pt alloy capsules, pressure media that include $BaCO_3$, salt, and talc, and experiments run in piston cylinders, 1 atm furnaces, and internally heated pressure vessels.

Models A and B (Table 4) were calibrated through multiple linear least-squares regression analysis using the program JMP, v. 4.0.4 (a product of the SAS institute). Several strategies were used in creating the models, and are similar to the approach used in Putirka (1999). First, t-ratios were checked for all variables; in general, we looked for t-ratios >5 and checked that our models achieved maximum values of the F-ratio, so as to avoid over-fitting the data [F-ratios are 426.1 for model A and 488.1 for model B of Table 4]. Next, each variable was checked using partial-regression leverage plots; variable coefficients that were controlled by just one or two experimental observations were considered suspect. Unless such variables led to an improvement in predicting values of T or P of the test data, either the data controlling such variables were removed from the calibration data set (and into the test data set), or the variables in question were eliminated from the model (or both). Finally, when several "candidate" models had been calibrated (usually having very similar F-ratios, but containing different variables), these models were compared on the basis of their ability to predict pressures and temperatures for the test data. For model reliability, we looked for models that exhibited the lowest standard error of estimate (SEE) on P and T for the data set as a whole, and whose regression slope and intercept for calculated vs. measured values most closely approached one and zero respectively. We also looked for decreases in SEE on mean values of P (with both reported and model temperatures as input), as well as increases in R^2, and improvements in the slopes and intercepts of regression lines through P(measured) vs. P(calculated) for mean calculated pressures. Finally, to check for systematic error and to ensure that the models covered all possible P-T-X_i dependencies, we compared model error to experimental T and P, and to the complete range of clinopyroxene and liquid compositions. Error for models A and B are uncorrelated with P, T, and all compositional variables, including f_{O2}, as noted above.

Results and discussion

Compared with the models presented in Putirka et al. (1996), the new expressions for the prediction of P and T (models A and B in Table 4) are somewhat more complex, but appear to reproduce T and P successfully for a very wide range of compositions. Although additional compositional corrections were required to describe the larger regression data set, and wider range of liquid compositions, model A yields errors on P (Fig. 2a) that are not much greater than for prior models (Putirka et al. 1996). Similarly, the error on model B (Fig. 2b) is not much larger than in Putirka et al. (1996), even though observed values of T in the present calibration range to about 200 K lower than in the prior study. The coefficients in (A) yield the following thermodynamic quantities: $\Delta H_r = -267$ kJ/mol, $\Delta S_r = -61.2$ J/(mol·K), and $\Delta V_r = -29.7$ cm^3/mol. These values are within a factor of 2 of 1 bar values for Jd crystallization, derived from calorimetric and partial molar volume studies (Lange and Carmichael 1987; Robie et al. 1979; Richet et al. 1993): $\Delta H_r = -154$ kJ/mol, $\Delta S_r = -113$ J/(mol·K), $\Delta V_r = -23.5$ cm^3/mol.

Models A and B also successfully reproduce pressures and temperatures for the test data set, which is composed of 407 experiments performed on a wide range of bulk compositions, and with experimental pressures ranging from 1 bar to 110 kbar (Fig. 3). Although model A systematically underestimates P at >50 kbar (largely representing experiments run in multi-anvil type apparatus), experimental pressures from 1 bar to 40 kbar are recovered without systematic offset, and an SEE of 4 kbar. The residuals of these test data are furthermore uncorrelated with P, T, or f_{O2} over the 1 bar–40 kbar range, and uncorrelated with all individual liquid and clinopyroxene compositional parameters over the entire pressure range, indicating that there is no systematic error, that no variables are missing from the model, and that model residuals represent experimental (and apparently random) error. As noted in Putirka et al. (1996), such error appears to result from phase heterogeneity rather than pressure mis-calibrations (see Putirka et al. 1996), and is probably related to the very slow diffusion rates in clinopyroxene. In an attempt to mitigate systematic error at P > 50 kbar, regression models were developed that included such data (from Putirka 1998 and Walter 1998), but such models over-estimate pressures on 1 bar experimental data. Because crystallization pressures are unlikely to often exceed 40 kbar for natural samples, and because accuracy is essential at low

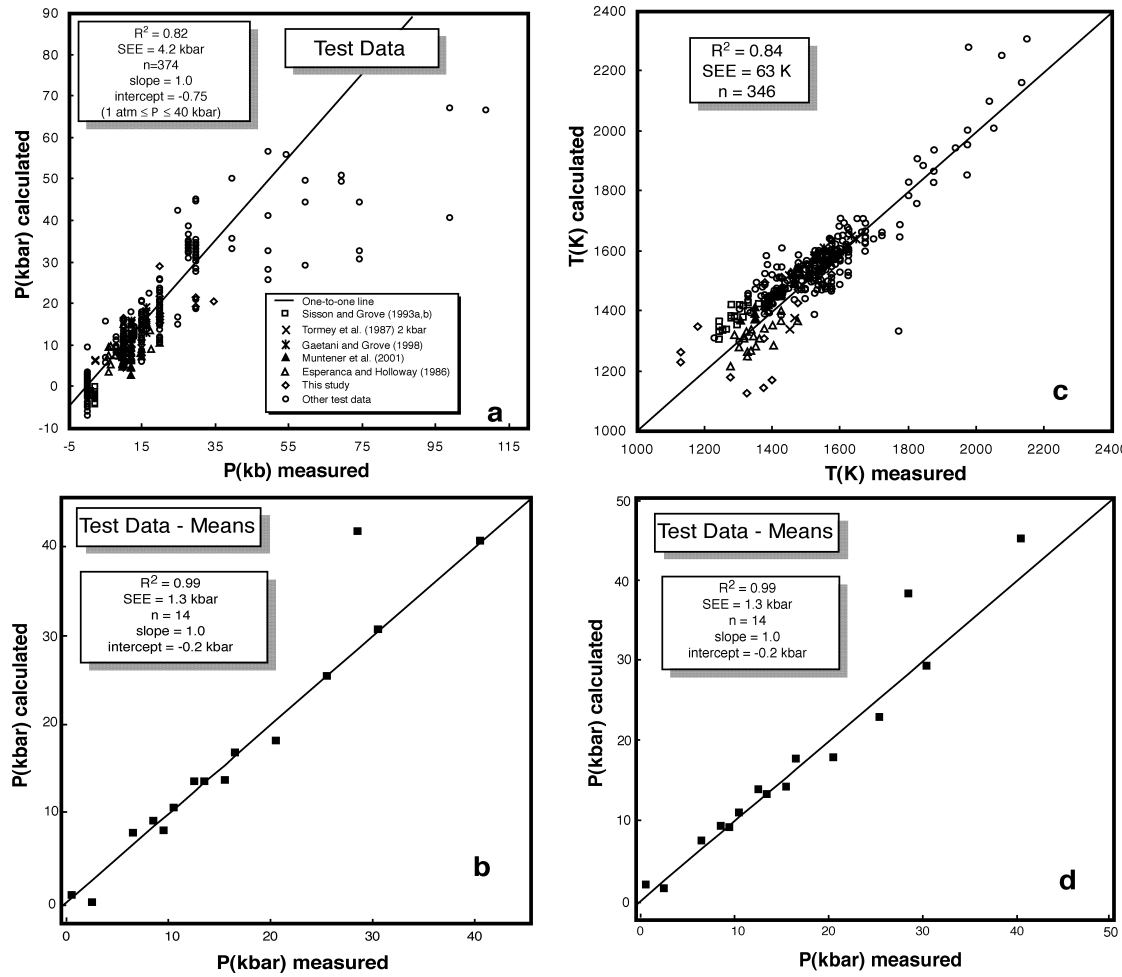

FIGURE 3. (**a**) Model A of Table 4 was used to calculate pressures for data that were not used for regression analysis, i.e., the "test data." Reported experimental temperatures were used as input. (**b**) Mean calculated pressures, using model A, are compared to reported experimental pressures. (**c**) Model B was used to calculate temperatures for the test data. (**d**) Models A and B were solved simultaneously to calculate both *P* and *T* for experimental data. Note that errors on mean calculated pressures are similar to the error in (**a**), where reported temperatures are used as input. Test data include 1 atm data from Juster et al. (1989), Kinzler (unpublished Ph.D. thesis, 1991), and Grove et al. (1992), and high-pressure data from: Bender et al. (1984), Fuji and Bougault (1983), Takahashi and Kushiro (1983), Esperança and Holoway (1986), Mahood and Baker (1986), Takahashi (1986), Tormey et al. (1987), Grove et al. (1990), Wei et al. (1990), Bartels et al. (1991), Kinzler and Grove (1992), Sisson and Grove (1993a, 1993b) Adam and Green (1994), Baker and Stolper (1994), Hack et al. (1994), Sen and Dunn (1994), Skulski et al. (1994), Blundy et al. (1995), Longhi (1995), Yang et al. (1996), Falloon et al. (1997), Kinzler (1997), Gaetani and Grove (1998), Kogiso et al. (1998), Nimis and Ulmer (1998), Putirka (1998), Robinson et al. (1998), Walter (1998), and Müntener et al. (2001).

pressure, such models were discarded.

Models A and B successfully reproduce pressures and temperatures for high-SiO_2 data from Esperança and Holloway (1986), and for hydrous data from Gaetani and Grove (1998) and Baker and Eggler (1987) (Fig. 3). As noted in Putirka et al. (1996), for those experimental studies in which several clinopyroxenes were analyzed and averaged for each experiment (e.g., Kinzler and Grove 1992), error on calculated pressures is greatly reduced. This observation suggests that clinopyroxenes approach equilibrium from random directions, and that, unsurprisingly, an average of multiple clinopyroxenes provides a more precise estimate of intensive variables compared to an individual analysis. Considering the test data as a whole, most experiments have been performed using similar basaltic bulk compositions, and are effectively "repeat" experiments. As in Putirka et al. (1996), we therefore calculated the mean value of calculated pressures for various isobaric data sets, and compared mean values to nominal pressure (Fig. 3b). With the exception of the 28 kbar data from Longhi (1995), mean values are very close to measured *P*, and the regression line through the means has a slope of unity and an intercept near zero (Fig. 3b). Furthermore, errors are not significantly greater when models A and B are solved simultaneously (as opposed to using reported values of *T* as input to model A) (Fig. 3d). All of these observations suggest that error is random and that model error, in practice, can perhaps be reduced to somewhat less than <1.5 kbar, provided that a sufficient number of pyroxenes are analyzed, and their *P* estimates averaged.

Hydrous basalts from Sisson and Grove (1993a, 1993b) and Müntener et al. (2001) also were used as test data, but model A yields pressures that are significantly below reported pressures for both data sets. The mean calculated pressure for the Sisson and Grove (1993a, 1993b) data are: –1.6 ± 0.5 kbar for the 1 kbar experiments, and –2.4 ± 1.1 kbar for the 2 kbar experiments. The mean calculated pressure for the Müntener et al. (2001) 12 kbar data is 7.0 ± 1.9 kbar. In contrast, the mean calculated pressure for the Baker and Eggler (1987) 2 kbar hydrous experiments is 1.6 ± 2.9 kbar. The reason for these discrepancies is unclear, and the models of Putirka et al. (1996) fare little better, with mean estimates of –3.5 and 6.3 kbar for the 2 kbar Sisson and Grove (1993a) and 12 kbar Müntener et al. (2001) data, respectively.

Unfortunately, all attempts to reduce error on the Sisson and Grove (1993a, 1993b) and Müntener et al. (2001) data were unsuccessful. We attempted to reconcile the low *P*-estimates by adding the Sisson and Grove (1993a, 1993b) and/or the Müntener et al. (2001) data into the regression models. All such efforts, though, yielded clearly inferior models, with systematically high pressure estimates for 1 atm experiments, and systematically low-*P* estimates for experiments performed at $P > 20$ kbar, for both the test and regression data sets. Indeed, with a mean calculated value of 3.6 ± 2.8 kbar, even the calculated pressures for the Baker and Eggler (1987) 2 kbar data were worse when the Sisson and Grove (1993a, 1993b) 2 kbar data are added to the regression model. (Our most successful effort at such a calibration is illustrated in Fig. 4).

In addition to our re-calibration of clinopyroxene-based thermobarometers, we also re-examined the equilibrium constant for Fe-Mg exchange between clinopyroxenes and co-existing liquids, $K_D^{\text{Fe-Mg}}$ [= $(Mg^{liq}Fe^{cpx})/(Mg^{cpx}Fe^{liq})$, where quantities such as Mg^{liq} represent mole or cation fractions of Mg in the liquid]. As with olivines (Roeder and Emslie 1970), $K_D^{\text{Fe-Mg}}$ can be extremely useful for the assessment at to whether natural clinopyroxenes have approached equilibrium with nominal liquid compositions. Values for $K_D^{\text{Fe-Mg}}$ from 440 experiments, which range from 850 to 1875 °C and from 0.001 to 110 kb, are distributed normally and, excluding data that lie beyond approximately 3σ, the range in $K_D^{\text{Fe-Mg}}$ is 0.105–0.488. The distribution has the following parameters: median = 0.267, mean = 0.275, standard deviation = 0.067, and standard error = 0.003. In a much smaller data set, Putirka (1998) presented a model to predict $K_D^{\text{Fe-Mg}}$ based on *P*, *T*, and several compositional parameters. In the larger data set examined here, inclusion of compositional parameters yields systematic error in calculated values of $K_D^{\text{Fe-Mg}}$ for the data set as a whole (as is evident also in Putirka 1998). For the assessment of equilibrium for natural clinopyroxenes, we suggest use of either a constant $K_D^{\text{Fe-Mg}}$ (i.e., model D in Table 4), or the temperature-sensitive formulation, model C, in Table 4 (Fig. 5).

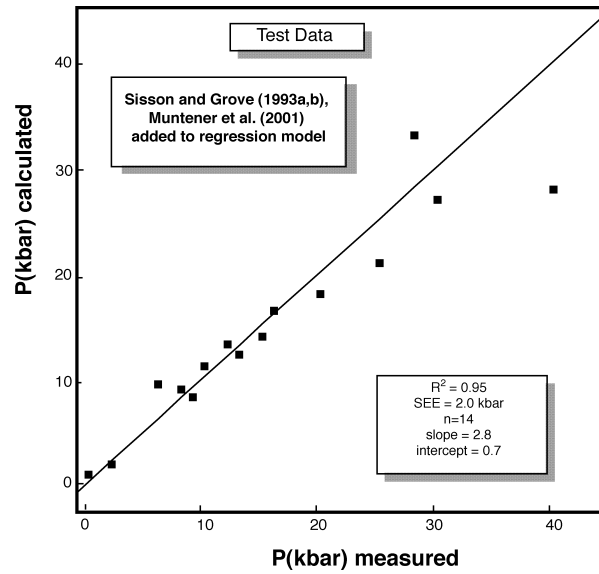

FIGURE 4. Data from Sisson and Grove (1993a, 1993b) and Müntener et al. (2001) were added to the regression data to obtain the following equation:

$$P(\text{kbar}) = 24.0 + 4.09\times10^{-3}T(K)\ln\left[\frac{[Jd^{cpx}]}{\left[Na^{liq}Al^{liq}\left(Si^{liq}\right)^2\right]}\right] + 14.1[Mg'^{liq}] - 363[Na^{liq}Al^{liq}] - 274.7[Ca^{liq}Si^{liq}] + 4.97\ln[Na^{liq}Al^{liq}]$$

This and other regression models that include these data underpredict *P* above 20 kbar, and slightly over-predict *P* for 1 atm experiments compared to models that exclude these data.

APPLICATIONS

Some of the most intriguing problems in magma transport concern the evolution and upward mobility of magmas in continental regions. Such lavas are often more silica rich and/or relatively hydrated compared to their oceanic counterparts. Their evolved nature is believed to be a result of fractionation and assimilation processes that occur when magmas stall during their transit to the surface (Eichelberger 1975; Hildreth and Moorbath 1988; Grove et al. 1988). However, we still have few constraints on the placement and physical controls of magma chamber formation.

To illustrate the application of the new thermobarometers to such issues, crystallization depths have been calculated for eruptive products from two continental localities: Neogene shoshonites from the Tibetan Plateau (Turner et al. 1996; Arnaud et al. 1992), and Neogene-Quternary basaltic to trachytic lavas from the eastern Snake River Plain (SRP), Idaho (Leeman 1974; Stout et al. 1994). Crystallization pressures and temperatures for these samples were calculated using models A and B, based on microprobe analyses of clinopyroxenes, and whole-rock analyses, which were used as nominal liquid compositions (Fig. 6).

Clearly, a crucial issue in such calculations is whether to select a whole rock, the matrix/glass composition, or some other composition (e.g., whole rock minus mass fraction of observed phenocryst phases) as representative of the liquid from which clinopyroxene phenocrysts have crystallized. At least two possible difficulties arise in such a selection. If clinopyroxenes form late in a crystallization sequence, the whole rock is unlikely to represent the liquid from which the clinopyroxenes have crystallized. Other mineralogic components would need to be subtracted from the whole rock (i.e., one could take the whole-rock composition, and subtract modal olivine), or clinopyroxene rims could be paired with matrix/glass compo-

sitions. If clinopyroxene is a liquidus phase, and the clinopyroxene mode is small, then a whole-rock composition could represent an equilibrium liquid, but only if the system, liquid + crystals, approximates a closed system during transport (i.e., no magma mixing or wall-rock assimilation following clinopyroxene crystallization). In the case of lavas from the SRP and Tibet, analyses of the rock matrix are unavailable, so we can only pair clinopyroxenes to whole-rock compositions in the present examples. Clearly some method is required to test whether these whole-rock compositions provide a valid match for a given clinopyroxene analysis.

The clinopyroxene saturation models of Putirka (1999) can be used to conduct just such a test. These models yield estimates of equilibrium clinopyroxene compositions (constrained from experiments) that can be compared to observed values for phenocrysts. To check whether whole rocks from the SRP and Tibet can be used as liquids, we calculated P and T from models A and B (using the whole-rock compositions), and input these values and the whole-rock compositions into the models of Putirka (1999; Table 3 of that paper). From Figure 7a, it is clear that at the calculated P-T conditions, only a few clinopyroxenes approach anticipated equilibrium compositions, even at the 2σ level, suggesting that only a subset of these P-T estimates are valid. We cannot determine from the Putirka (1999) saturation models whether such clinopyroxenes are xenocrysts, or whether the liquid compositions have been dis-

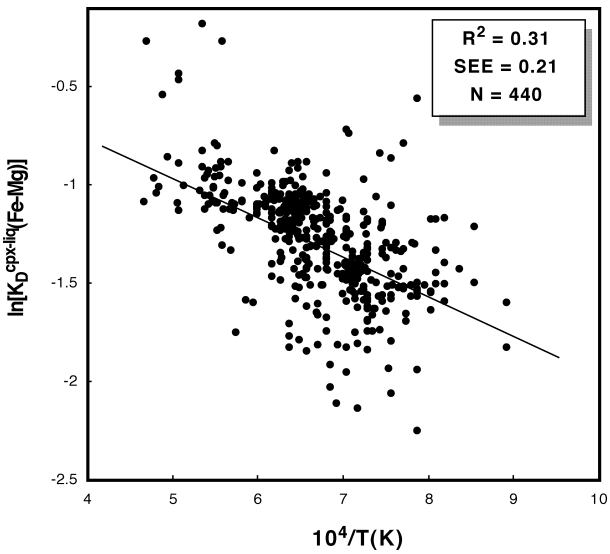

FIGURE 5. $\ln(K_D^{Fe\text{-}Mg})$ v. $10^4/T(K)$ [where $K_D^{Fe\text{-}Mg} = (MgO^{liq}FeO^{cpx})/(MgO^{cpx}FeO^{liq})$], $K_D^{Fe\text{-}Mg}$, although nearly constant, is somewhat sensitive to T. A regression line (model C of Table 4) is illustrated; data outside the 3σ range for the mean $K_D^{Fe\text{-}Mg}$ are excluded.

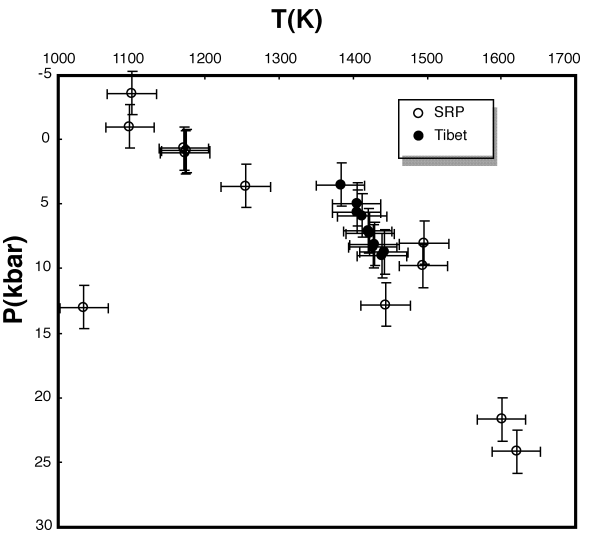

FIGURE 6. Models A and B (Table 4) were used to calculate crystallization pressures and temperatures for clinopyroxene-bearing lavas from the Tibetan Plateau (Arnaud et al. 1992; Turner et al. 1996) and the eastern Snake River Plain (Leeman 1974; Stout et al. 1994).

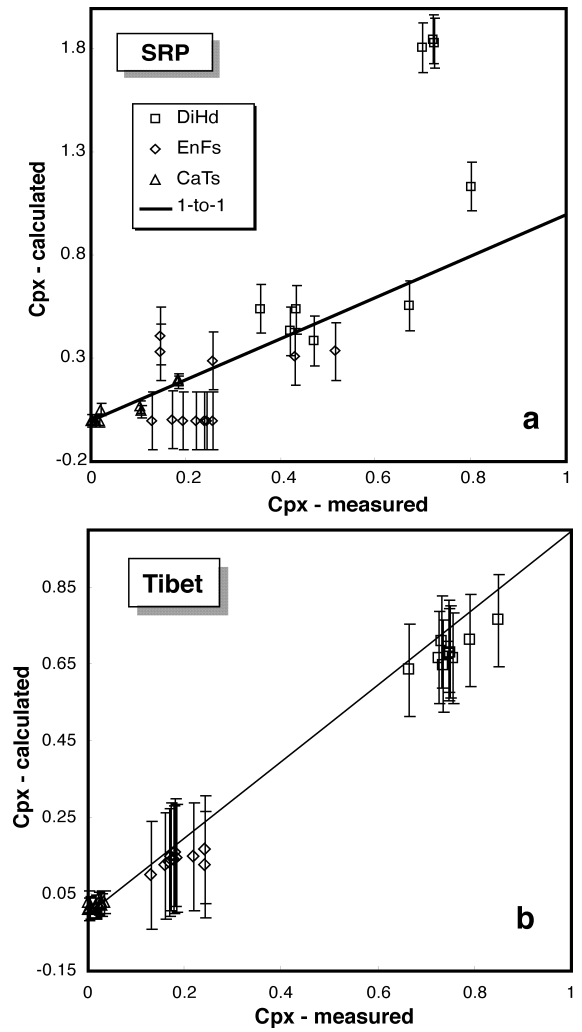

FIGURE 7. Observed clinopyroxene compositions are compared to calculated compositions using models 3.1–3.7 of Putirka (1999) for the SRP (**a**) and Tibet (**b**); P-T estimates from models A and B are used as input. Error bars on the calculated pyroxene components, DiHd and EnFs (enstatite + ferrosilite), represent twice the standard error of estimate of the models of Putirka (1999), i.e., a 2σ error.

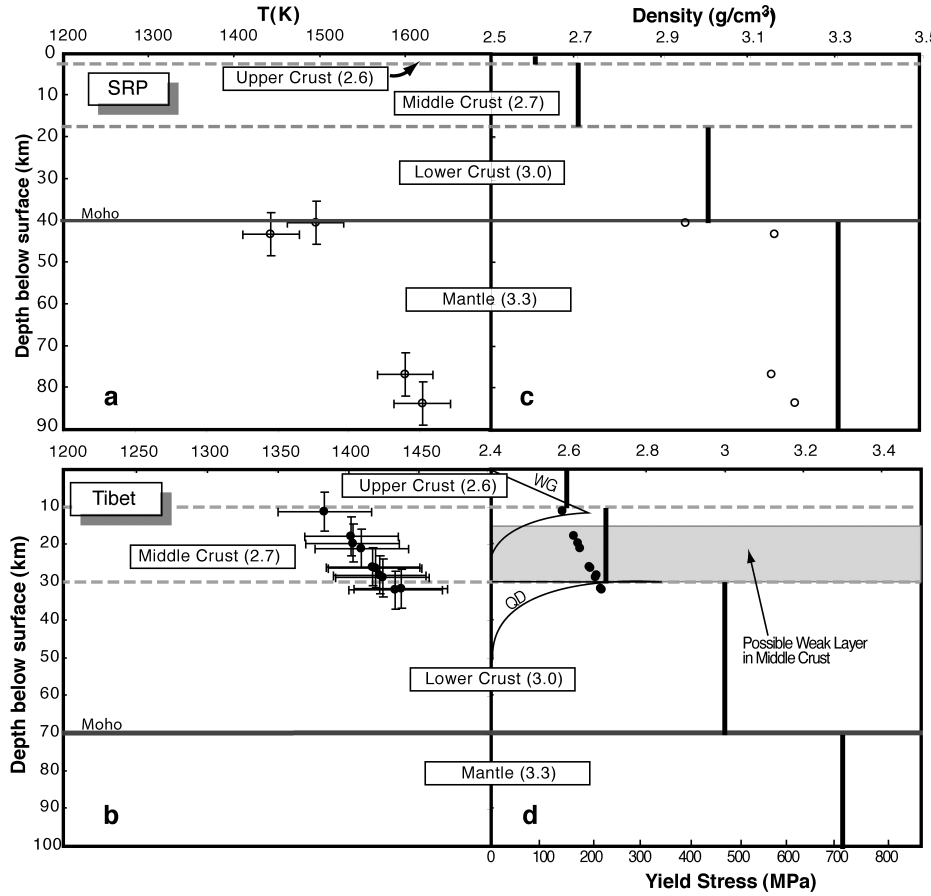

FIGURE 8. For the subset of clinopyroxenes that approach nominal equilibrium values (Fig. 6), pressure estimates were converted to depths for lavas from the SRP (**a**) and Tibet (**b**). In both regions, the following crust and lithosphere densities were used to convert pressures to depths: upper crust, 2.6 g/cm^3; middle crust, 2.7 g/cm^3; lower crust, 3.0 g/cm^3; mantle 3.3 g/cm^3. Thicknesses for upper, middle, and lower crust in the SRP were taken as: 2, 16, and 22 km; for Tibet, thicknesses of 10, 20, and 40 km were used. Maximum interpolation errors on depth are less than 0.5 km in both cases. In (**c**) and (**d**), crystallization depths are compared to crust and magma densities (magma densities were calculated using partial molar volumes of liquid components, and their respective values for dV/dT and dV/dP from Lange and Carmichael 1987); crustal densities are shown as dark vertical lines, and in parentheses. Yield-strength curves (adapted from Dunbar and Sawyer 1989) for wet granite (WG) and quartz diorite (QD) illustrate potential weak layers within the crust.

turbed by mixing or post-clinopyroxene crystallization (though petrographic and geochemical tests could be used to decipher such issues). Nonetheless, these models allow us to filter only those clinopyroxene-whole rock pairs whose compositions are consistent with experimental constraints on clinopyroxene-melt equilibrium. And just as whole rocks were tested in Figure 7a, any other nominal melt composition, such as matrix glass, if such data were available, could be tested similarly. In our discussion below, only those samples that yielded apparent equilibrium clinopyroxene-liquid pairs (i.e., that match within 2σ) are considered further.

As an interesting counterpoint to the SRP, clinopyroxenes from Tibetan shoshonites match closely with calculated equilibrium values (Fig. 7b), suggesting that: (1) the reported whole-rock compositions closely approximate the liquids from which clinopyroxene phenocrysts crystallized; and (2) that the *P-T* conditions estimated using models A and B are consistent with experimentally constrained clinopyroxene-saturation conditions, and thus are probably valid.

To illustrate how such depth estimates can be used to address various geological problems, crystallization depths are converted from pressure estimates based on reported density profiles (Wittlinger et al. 1996; Molnar 1988; Smith and Braile 1994) (Fig. 8), and compared to density and strength profiles of the crust. As the data sets are small, no secure conclusions can, of course, be drawn, but the regional contrasts of crystallization depths are nevertheless interesting. Whereas SRP lavas would appear to be neutrally buoyant in the lower crust (based on magma densities calculated using expressions from Lange and Carmichael 1987), SRP lavas apparently can be transported from much greater depths (Figs. 8a and 8c), suggesting that the Moho is not a significant barrier to transport. In contrast, depth estimates from Tibet (Fig. 8b) lie mostly within the middle crust. Calculated magma densities for Tibetan lavas suggest that the middle crust may act as a level of neutral buoyancy for primitive magmas, and that stagnation and differentiation within

the middle crust may be required for such magmas prior to their ascent to the surface (Fig. 8d). These observations tentatively indicate that density contrasts within the middle crust, rather than at the Moho, may influence magma transport. But it also appears that at least some magmas in the SRP are transported through crustal layers with much lower density.

In addition to a density control, it also has been proposed that rheology of the crust can control magma transport (Gans et al. 1989; Parsons et al. 1992; Putirka 1997). To test this idea for Tibet, we plotted yield strength curves in Figure 8d, as adapted from Dunbar and Sawyer (1989). According to this figure, it appears that crystallization depths are at least consistent with stagnation within a weak middle crust. Indeed, most Tibetan magmas appear to be at least slightly less dense than the middle crust. The data are too few to yield a decisive result, but it could be argued that a decreased density contrast and a weak middle crust both contribute to magma stagnation.

In both the SRP and Tibet, it is clear that magmas can bypass low-density layers, such as the upper crust. One reason for such an effect is the varying ability of fractures to cut their way to the surface. Dike size and aspect ratio should control magma transport through fractures. The stress at a crack tip, σ, may be approximated by $\sigma = \sigma_r(1 + 2h/w)$, where σ_r = remote stress, h = dike half-height, and w = dike half-width (Scholz 1990). Stress intensity is therefore greater for cracks with a greater h/w ratio. For a given width, dikes with a greater depth extent not only will be more buoyant, but also will have a greater ability to cut their way through low density layers. In addition, as discussed by Lister and Kerr (1991), dikes that are deeply rooted in high-density material are likely to be positively buoyant overall, even if a portion of the dike is surrounded by low-density material. Returning to our examples, SRP magmas appear to have sufficient buoyancy (size) to be transported past potential rheologic boundaries and shallow-level density contrasts that might otherwise impede upward mobility.

ACKNOWLEDGMENTS

We thank Ian Hutcheon at LLNL and Michael Jercinovic at UMA for their help with use of their respective electron microprobe facilities, and Nick Arnaud for donating the shoshonite bulk compositions used in this study. This paper benefited greatly from thoughtful reviews by Bill Minarik, Kevin Righter, and an anonymous reviewer. This work was supported by LLNL.

REFERENCES CITED

Adam, J. and Green, T.H. (1994) The effects of pressure and temperature on the partitioning of Ti, Sr and REE between amphibole, clinopyroxene and basanitic melts. Chemical Geology, 117, 219–233.

Arnaud, N.O., Vidal, Ph., Tapponnier, P., Matte, Ph., and Deng, W.M. (1992) The high K_2O volcanism of northwestern Tibet: Geochemistry and tectonic implications. Earth and Planetary Science Letters, 111, 351–367.

Baker, D.R. and Eggler, D.H. (1987) Compositions of anhydrous and hydrous melts coexisting with plagioclase, augite, and olivine or low-Ca pyroxene from 1 atm to 8 kbar: application to the Aleutian volcanic center of Atka. American Mineralogist, 72, 12–28.

Baker, M.B. and Stolper, E.M. (1994) Determining the composition of high-pressure mantle melts using diamond aggregates. Geochimica et Cosmochimica Acta, 58, 2811–2827.

Bartels, K.S., Kinzler, R.J., and Grove, T.L. (1991) High pressure phase relations of primitive high-alumina basalts from Medicine Lake volcano, northern California. Contributions to Mineralogy and Petrology, 108, 253–270.

Bender, J.F., Langmuir, C.H., and Hanson, G.N. (1984) Petrogenesis of basalt glasses from the Tamayo Region, East Pacific Rise. Journal of Petrology, 25, 213–254.

Blundy, J.D., Falloon, T.J., Wood, B.J., and Dalton, J.A. (1995) Sodium partitioning between clinopyroxene and silicate melts. Journal of Geophysical Research, 100, 15501–15515.

Dixon, J.E., Stolper, E.M., and Holloway, J.R. (1995) An experimental study of water and carbon dioxide solubilities in mid-ocean ridge basaltic liquids. Part 1: Calibration and solubility models. Journal of Petrology, 36, 1607–1631.

Dunbar, J.A. and Sawyer, D.S. (1989) How preexisting weaknesses control the style of continental breakup. Journal of Geophysical Research, 94, 7278–7292.

Dvorak, J.J. and Dzurisin, D. (1993) Variations in magma supply rate at Kilauea volcano, Hawaii. Journal of Geophysical Research, 98, 22255–22268.

Dvorak, J.J., Okamura, A.T., and Dieterich, J.H. (1983) Analysis of surface deformation data, Kilauea volcano, Hawaii, October 1966 to September 1970. Journal of Geophysical Research, 88, 9295–9304.

Eichelberger, J.C. (1975) Origin of andesite and dacite: evidence of mixing at Glass Mountain, in California, and other circum-Pacific volcanoes. Geological Society of America Bulletin, 86, 1381–1391.

Esperança, S. and Holoway, J.R. (1986) The origin of the high-K latities from Camp Creek Arizona: constraints from experiments with vπariable f_{O_2} and aH_2O. Contributions to Mineralogy and Petrology, 93, 504–512.

Falloon, T.J., Green, D.H., O'Neill, H.St.C., and Hibberson, W.O. (1997) Experimental tests of low degree peridotite partial melt compositions; implications for the nature of anhydrous near-solidus peridotite melts at 1 GPa. Earth and Planetary Science Letters, 152, 149–162.

Fram, M.S. and Longhi, J. (1992) Phase equilibria of dikes associated with Proterozoic anorthosite complexes. American Mineralogist, 77, 605–616.

Fuji, T. and Bougault, H. (1983) Melting relations of a magnesian abyssal tholeiite and the origin of MORBs. Earth and Planetary Science Letters, 62, 283–295.

Gaetani, G.A and Grove, T.L. (1998) The influence of water on melting of mantle peridotite. Contributions to Mineralogy and Petrology, 131, 323–346.

Gans, P.B., Mahood, G.A., and Schermer, E. (1989) Synextensional magmatism in the Basin and Range Province; a case study from the eastern Great Basin. Geological Society of America Special Paper 233, 53 p.

Ghiorso, M.S. and Sack, R.O. (1995) Chemical mass transfer in magmatic processes IV. A revised and internally consistent thermodynamic model for the interpolation and extrapolation of liquid-solid equilibria in magmatic systems at elevated temperatures and pressures. Contributions to Mineralogy and Petrology, 119, 197–212.

Ghiorso, M.S., Hirschmann, M.M., Reiners, P.W., and Kress, V.C. III (2002) The pMELTS: a revision of MELTS for improved calculation of phase relations and major element partitioning related to partial melting of the mantle to 3 GPa. Geochemistry, Geophysics, Geosystems, 3, 1–36, 10.1029/2001GC000217.

Grove, T.L. and Juster, T.C. (1989) Experimental investigations of low-Ca pyroxene stability and olivine-pyroxene-liquid equilibria at 1-atm in natural basaltic and andesitic liquids. Contributions to Mineralogy and Petrology, 103, 287–305.

Grove, T.L., Kinzler, R.J., Baker, M.B., Donnelly-Nolan, J.M., and Lesher, C.E. (1988) Assimilation of granite by basaltic magma at Burnt Lava flow, Medicine Lake volcano, northern California: decoupling of heat and mass transfer. Contributions to Mineralogy and Petrology, 99, 320–343.

Grove, T.L., Kinzler, R.J., and Bryan, W.B. (1990) Natural and experimental phase relations of lavas from Serocki Volcano. Proceedings of the Ocean Drilling Program, Scientific Results, 106/109, 9–17.

——— (1992) Fractionation of mid-ocean ridge basalt (MORB). In J. Phipps Morgan, D.K. Blackman, and J.M. Sinton, Eds., Mantle flow and melt generation at mid ocean ridges, p. 281–310. Geophysical Monograph Series, 7, AGU, Washington, D.C.

Gudmundsson, A. (1986) Formation of crustal magma chambers in Iceland. Geology, 14, 164–166.

Guetschow, H.A. and Nelson, B.K. (2002) Shallow fractionation signature of phase chemistry in Taburiente lavas, La Palma, Canary Islands: results of MELTS modeling. EOS, Transactions of the American geophysical Union, 83, F1418.

Hack, P.J., Nielsen, R.L., and Johnston, A.D. (1994) Experimentally determined rare-earth element and Y partitioning behavior between clinopyroxene and basaltic liquids at pressures up to 20 kbar. Chemical Geology, 117, 89–105.

Halbach, H. and Chatterjee, N.D. (1982) An empirical Redlich-Kwong-type equation of state for water to 1,000°C and 200 Kbar. Contributions to Mineralogy and Petrology, 79, 337–345.

Hansteen, T.H., Klugel, A., and Schminke, H-U. (1998) Muli-stage magma ascent beneath the Canary Islands: evidence from fluid inclusions. Contributions to Mineralogy and Petrology, 132, 48–64.

Hermann, J., Müntener, O., and Gunther, D. (2001) Differentiation of mafic magma in a continental crust-to-mantle transition zone. Journal of Petrology, 42, 189–206.

Hildreth, W. and Moorbath, S. (1988) Crustal contributions to arc magmatism in the Andes of Central Chile. Contributions to Mineralogy and Petrology, 98, 455–489.

Holloway, J.R. (1977) Fugacity and activity of molecular species in supercritical fluids. In D.G. Fraser, Ed., Thermodynamics of Geology, p. 161–181. Reidel Publishing, Dordrecht, Holland.

Holloway, J.R., Pan, V., and Gudmundsson, G. (1992) High pressure fluid-absent experiments in the presence of graphite: oxygen fugacity, ferric/ferrous ratio and dissolved CO_2. European Journal of Mineralogy, 4, 105–114.

Hooft, E.E. and Detrick, R.S. (1993) The role of density in the accumulation of basaltic melts at mid-ocean ridges. Geophysical Research Letters, 20, 423–426.

Juster, T.C., Grove, T.L., and Perfit, M.R. (1989) Experimental constraints on the generation of FeTi basalts, andesites and rhyodacites at the Galapagos Spread-

ing center, 85°W and 95°W. Journal of Geophysical Research, 94, 9251–9274.
Kinzler, R.J. (1991) Experimental constraints on the generation and evolution of mid-ocean ridge basalts. Unpublished Ph.D. Thesis, MIT, 244 p.
——— (1997) Melting of mantle peridotite at pressures approaching the spinel to garnet transition: Application to mid-ocean ridge basalt petrogenesis. Journal of Geophysical Research, 102, 853–874.
Kinzler, R.J. and Grove, T.L. (1992) Primary magmas of mid-ocean ridge basalts 1. Experiments and methods. Journal of Geophysical Research, 97, 6885–6906.
Kilinc, A.I., Locke, D.R., Dogan, U., and Dogan, M. (1999) An AFC model for the meso- and neo-volcanics of the Hasan Dagi Complex, central Anatolia, Turkey. Geological Society of America Annual Meeting, Abstract with Program, 31, 478.
Klein, C. (2001) Mineral Science. 22nd ed., 641 p. Wiley, New York.
Kogiso, T., Hirose, K., and Takahashi, E. (1998) Melting experiments on homogeneous mixtures of peridotite and basalt: application to the genesis of ocean island basalts. Earth and Planetary Science Letters, 162, 45–61.
Kolsrud, T., Miller, C.F., and Thomas, C.W. (2001) Lake Chatuge revisited; crystallization in a shallow oceanic magma chamber. Geological Society of America, Southeastern Section, Abstracts with Programs, 33, 2–3.
Kuntz, M. (1992) A model-based perspective of basaltic volcanism, eastern Snake River Plain, Idaho. In P.K. Link, M.A. Kuntz, and L.B. Plat, Eds., Regional geology of eastern Idaho and western Wyoming, p. 289–304. Geological Society of America Memoir 179, Boulder, CO.
Lange, R.A. and Carmichael, I.S.E. (1987) Densities of Na_2O-K_2O-CaO-FeO-Fe_2O_3-Al_2O_3-TiO_2-SiO_2 liquids: new measurements and derived partial molar properties. Geochimica et Cosmochimica Acta, 51, 2931–2946.
Leeman, W.P. (1974) Petrology of basaltic lavas from the Snake River Plain, Idaho. Unpublished Ph.D. thesis, University of Oregon, 337 p.
Lister, J.R. and Kerr, R.C. (1991) Fluid-mechanical models of crack propagation and their application to magma transport in dykes. Journal of Geophysical research, 96, 10049–10077.
Lindsley, D.H. (1983) Pyroxene thermometry. American Mineralogist, 68, 477–493.
Longhi, J. (1995) Liquids equilibria of some primary lunar and terrestrial melts in the garnet stability field. Geochimica et Cosmochimica Acta, 59, 2375–2386.
MacDonald, G.A. and Katsura, T. (1965) Eruption of Lassen Peak, Cascade Range, California, in 1915: example of mixed magmas. Geological Society of America Bulletin. 76, 475–482.
Mahood, G.A. and Baker, D.R. (1986) Experimental constraints on depths of fractionation of mildly alkalic basalts and associated felsic rocks; Pantelleria, Strait of Sicily. Contributions to Mineralogy and Petrology, 93, 251–264.
McGuire, A.V., Dyar, M.D., and Ward, K. (1989) Neglected Fe^{3+}/Fe^{2+} ratios—a study of Fe^{3+} content of megacrysts from alkali basalts. Geology, 17, 687–690.
Molnar, P. (1988) A review of geophysical constraints on the deep structure of the Tibetan Plateau, the Himalaya and the Karakoram, and their tectonic implications. Philosophical Transactions of the Royal Society of London, Series A, 326, 33–88.
Moore, G., Vennemann, T., and Carmichael, I.S.E. (1998) An empirical model for the solubility of H_2O in magmas to 3 kilobars. American Mineralogist, 83, 36–42.
Müntener, O., Kelemen, P.B., and Grove, T.L. (2001) The role of H_2O during crystallization of primitive arc magmas under uppermost mantle conditions and genesis of igneous pyroxenites: an experimental study. Contributions to Mineralogy and Petrology, 141, 643–658.
Navin, D.A., Pierce, C., and Sinha, M.C. (1998) The RAMESSES experiment II evidence for accumulated melt beneath a slow spreading ridge from wide-angle refraction and multichannel reflection and seismic profiles. Geophysical Journal International, 135, 746–772.
Nielsen, R.L. and Drake, M.J. (1979) Pyroxene-melt equilibria. Geochimica et Cosmochimica Acta, 43, 1259–1272.
Nimis, P. (1995) A clinopyroxene geobarometer for basaltic systems based on crystal-structure modeling. Contributions to Mineralogy and Petrology, 121, 115–125.
——— (1999) Clinopyroxene geobarometry of magmatic rocks. Part 2. Structural geobarometers for basic to acid, tholeiitic and mildly alkaline magmatic systems. Contributions to Mineralogy and Petrology, 135, 62–74.
Nimis, P. and Ulmer, P. (1998) Clinopyroxene geobarometry of magmatic rocks part 1: An expanded structural geobarometer for anhydrous and hydrous, basic and ultrabasic systems. Contributions to Mineralogy and Petrology, 133, 122–135.
Parsons, T. and Thompson, G.A. (1993) Does magmatism influence low-angle normal faulting? Geology, 21, 247–250.
Parsons, T., Howie, J.M., and Thompson, G.A. (1992) Seismic constraints on the nature of the lower crustal reflectors beneath the extending southern transition zone of the Colorado Plateau, Arizona. Journal of Geophysical Research, 97, 12391–12407.
Putirka, K. (1997) Magma Transport at Hawaii: Inferences based on igneous thermobarometry. Geology, 25, 69–72.
——— (1998) Garnet + liquid equilibrium. Contributions to Mineralogy and Petrology, 131, 273–288.
——— (1999) Clinopyroxene + liquid equilibria to 100 kbar and 240 K. Contributions to Mineralogy and Petrology. 135, 151–163.
Putirka, K., Johnson, M., Kinzler, R., Longhi, J., and Walker, D. (1996) Thermobarometry of mafic igneous rocks based on clinopyroxene-liquid equilibria, 0-30 kb. Contributions to Mineralogy and Petrology, 123, 92–108.
Richet, P., Robie, R.A., and Hemingway, B.S. (1993) Entropy and structure of silicate glasses and melts. Geochimica et Cosmochimica Acta, 57, 2751–2766.
Robie, R.A., Hemingway, B.S., and Fisher, J.R. (1979) Thermodynamic properties of minerals and related substances at 298.15 K and 1 bar (10^5 Pascals) pressure and at higher temperatures. Geological Survey Bulletin 1452, 456 p.
Robinson, J.A.C., Wood, B.J., and Blundy, J.D. (1998) The beginning of melting of fertile and depleted peridotite at 1.5 GPa. Earth and Planetary Science Letters, 155, 97–111.
Roeder, P.L. and Emslie, R.F. (1970) Olivine-liquid equilibrium. Contributions to Mineralogy and Petrology, 29, 275–289.
Ryan, M.P. (1987) Neutral buoyancy and the mechanical evolution of magmatic systems. In B.O. Mysen, Ed., Magmatic Processes: Physiochemical Principles, p. 259–287. The Geochemical Society, University Park, Texas.
Salvioli, M.E., Mattioloi, M., Rensulli, A., and Serri, G. (2002) Silicate melt inclusions in the cumulate minerals of gabbroic nodules from Stromboli Volcano (Aeolian Islands, Italy); main components of the fluid phase and crystallization temperatures. Mineralogical Magazine, 66, 969–984.
Scholz, C.H. (1990) The Mechanics of Faulting. Cambridge University Press, NY, NY, 439 p.
Sen, C. and Dunn, T. (1994) Dehydration melting of a basaltic composition amphibolite at 1.5 and 2.0 GPa; implications for the origin of adakites. Contributions to Mineralogy and Petrology, 117, 394–409.
Shaw, H.R. (1980) The fracture mechanisms of magma transport from the mantle to the surface. In R.B. Hargraves, Ed., Physics of magmatic processes, p. 201–264. Princeton University Press.
Sisson, T.W. and Grove, T.L. (1993a) Experimental investigations of the role of H_2O in calc-alkaline differentiation and subduction zone magmatism. Contributions to Mineralogy and Petrology, 113, 143–166.
——— (1993b) Temperatures and H_2O contents of low-MgO high-alumina basalts. Contributions to Mineralogy and Petrology, 113, 167–184.
Skulski, T., Minarik, W., and Watson, E.B. (1994) High-pressure experimental trace-element partitioning between clinopyroxene and basaltic melts. Chemical Geology, 117, 127–147.
Smith, R.B. and Braile, L.W. (1994) The Yellowstone hotspot. Journal of Volcanology and Geothermal Research, 61, 121–187.
Stolper, E. and Walker, D. (1980) Melt density and the average composition of basalt. Contributions to Petrology and Mineralogy, 74, 7–12.
Stout, M.Z., Nicholls, J., and Kuntz, M.A. (1994) Petrological and mineralogical variations in 2500-2000 yr B.P. lava flows, Craters of the Moon Lava Field, Idaho. Journal of Petrology, 35, 1681–1715.
Takahashi, E. (1986) Melting of a dry peridotite KLB-1 up to 14 GPa: implications on the origin of peridotitic upper mantle. Journal of Geophysical Research, 91, 9367–9382.
Takahashi, E. and Kushiro, I. (1983) Melting of a dry peridotite at high pressures and basalt magma genesis. American Mineralogist, 68, 859–879.
ten Brink, U.S. and Brocher T.M. (1987) Multichannel seismic evidence for a subcrustal intrusive complex under Oahu and a model for Hawaiian volcanism, Journal of Geophysical Research, 92, 13687–13707.
Tormey, D.R., Grove, T.L., and Bryan, W.B. (1987) Experimental petrology of normal MORB near the Kane Fracture Zone: 22°–25° N, mid-Atlantic Ridge. Contributions to Mineralogy and Petrology, 96, 121–139.
Trua, T., Serri, G., Marani, M., Renzulli, A., and Gamberi, F. (2002) Volcanological and petrological evolution of Marsili Seamount (southern Tyrrhenian Sea). Journal of Volcanology and Geothermal Research, 114, 441–464.
Turner, S., Arnaud, N., Liu, J., Rogers, N., Hawkesworth, C., Harris, N., Kelley, S., van Calsteren, P., and Deng, W. (1996) Post-collision, shoshonitic volcanism on the Tibetan Plateau: Implications for convective thinning of the lithosphere and the source of Ocean Island Basalts. Journal of Petrology, 37, 45–71.
Walter, M.J. (1998) Melting of garnet peridotite and the origin of komatiite and depleted lithosphere. Journal of Petrology, 39, 29–60.
Walter, M.J. and Presnall, D.C. (1994) Melting behavior of simplified lherzolite in the system CaO-MgO-Al_2O_3-SiO_2-Na_2O from 7 to 35 kbar. Journal of Petrology, 35, 329–359.
Wei, K., Tronnes, R.G., and Scarfe, C.M. (1990) Phase relations of aluminum-undepleted and aluminum-depleted komatiites at pressures of 4-12 GPa. Journal of Geophysical Research, 95, 15817–15827.
Wittlinger, G. Masson, F., Poupinet, G., Tapponnier, P., Mei, J., Herquel, G., Guilbert, J., Achauer, U., Guanqi, X., Danian, S., and Lithoscope Kinlun Team (1996) Seismic tomography of northern Tibet and Kunlun: evidence for crustal blocks and mantle velocity contrasts. Earth and Planetary Science Letters, 139, 263–279.
Yang, H-J., Kinzler, R.J., and Grove, T.L. (1996) Experiments and models of anhydrous, basaltic olivine-plagioclase-augite saturated melts from 0.001 to 10 kbar. Contributions to Mineralogy and Petrology, 124, 1–18.
Yang, H-J., Frey, F.A., Clague, D.A., and Garcia, M.O. (1999) Mineral chemistry of submarine lavas from Hilo Ridge, Hawaii; implications for magmatic processes within Hawaiian rift zones. Contributions to Mineralogy and Petrology, 135, 355–372.

MANUSCRIPT RECEIVED OCTOBER 8, 2002
MANUSCRIPT ACCEPTED JUNE 2, 2003
MANUSCRIPT HANDLED BY KEVIN RIGHTER